Inversion of azimuthally dependent NMO velocity in transversely isotropic media with a tilted axis of symmetry

Vladimir Grechka & Ilya Tsvankin

ABSTRACT

Just as the transversely isotropic model with a vertical symmetry axis (VTI media) is typical for horizontally layered sediments, transverse isotropy with a tilted symmetry axis (TTI) describes *dipping* TI layers, such as uptilted shale beds near salt domes. Here, we show that all parameters of TTI media responsible for P-wave velocity, including the tilt and azimuth of the symmetry axis, can be obtained from azimuthally-varying P-wave normal-moveout (NMO) velocities measured for two reflectors with different dips and/or azimuths (one of the reflectors can be horizontal). The shear-wave velocity V_{S0} in the symmetry direction, which has negligible influence on P-wave kinematic signatures, can be found only from the moveout of SV-waves.

Using the exact NMO equation, we examine the propagation of errors in observed moveout velocities into estimated values of the anisotropic parameters and establish the necessary conditions for a stable inversion procedure. Since the azimuthal variation of the NMO velocity has been shown to be elliptical, each reflection event provides us with up to three constraints on the model parameters. P-wave NMO velocity in TTI media is controlled by the velocity V_{P0} in the symmetry direction, Thomsen's anisotropic coefficients ϵ and δ, and the orientation (tilt ν and azimuth β) of the symmetry axis. Generally, all five parameters can be obtained from two P-wave NMO ellipses, but the feasibility of the moveout inversion strongly depends on the tilt ν. If the symmetry axis is close to vertical (small ν), the P-wave NMO ellipse is largely governed by the NMO velocity from a horizontal reflector $V_{P\mathrm{nmo}}(0)$ and the "anellipticity" coefficient η, which is close to the difference between ϵ and δ; in this case, the parameters ϵ and δ cannot be determined separately. Only if the tilt exceeds 30-40° (e.g., the symmetry axis can be horizontal), it is possible to resolve all P-wave moveout parameters individually. Another condition required for a stable parameter estimation is that the medium be sufficiently different from elliptical (i.e., ϵ cannot be close to δ). This limitation, however, can be overcome by including the SV-wave NMO ellipse from a horizontal reflector in the inversion procedure.

Although most of the analysis is carried out for a single TTI layer, we extend the inversion algorithm to vertically heterogeneous TTI media above a dipping reflector using the generalized Dix equation. A synthetic example for a strongly anisotropic, stratified TTI medium demonstrates a high accuracy of the inversion for models with sufficient tilt of the symmetry axis. The results of moveout inversion in TTI media are sufficient for performing anisotropic *depth* imaging, as opposed to *time* imaging for vertical transverse isotropy.

Introduction

Transverse isotropy (TI) is the most common anisotropic model of the subsurface typical for massive shale formations or thin-bed sedimentary sequences. If sediments are horizontally layered, the symmetry axis of the corresponding TI medium is vertical (the so-called VTI model, or vertical transverse isotropy). For dipping TI layers, often found in overthrust areas or near flanks of

salt domes and volcanic intrusions, the symmetry axis usually remains orthogonal to the layering and, therefore, becomes tilted (TTI media). TI media with a horizontal (HTI) or near-horizontal symmetry axis are often associated with vertical or steeply dipping fracture systems (e.g., Thomsen, 1988).

Reflection traveltime, in general, and normal-moveout (NMO) velocity, in particular, provide the most reliable information about the anisotropic parameters of TI media. For vertical transverse isotropy, as shown by Alkhalifah and Tsvankin (1995), P-wave NMO velocity in the dip plane of the reflector (and time-domain processing as a whole) are controlled by only *two* parameter combinations: the zero-dip NMO velocity (i.e., the NMO velocity for a horizontal reflector)

$$V_{P\mathrm{nmo}}(0) = V_{P0}\sqrt{1+2\delta}\,, \tag{1}$$

and the anisotropic parameter

$$\eta = \frac{\epsilon-\delta}{1+2\delta}\,. \tag{2}$$

Here V_{P0} is the P-wave velocity in the symmetry (vertical) direction, and ϵ and δ are Thomsen's (1986) anisotropic coefficients; V_{P0}, ϵ and δ are responsible for all P-wave kinematic signatures in VTI media (Tsvankin, 1996). The parameter η goes to zero in elliptically anisotropic media ($\epsilon=\delta$) and, therefore, describes the "anellipticity" of the P-wave slowness surface. For elliptical anisotropy, normal-moveout velocity is the same function of the ray parameter p and zero-dip NMO velocity as in isotropic media. Provided $V_{P\mathrm{nmo}}(0)$ has been obtained using semblance analysis of horizontal events, η can be estimated from the NMO velocity for a dipping reflector.

The result of Alkhalifah and Tsvankin (1995) was based on the 2-D NMO equation of Tsvankin (1995) restricted to a common-midpoint (CMP) line in the dip plane of the reflector. Grechka and Tsvankin (1996) developed a more general 3-D NMO equation valid for CMP reflections recorded over arbitrary anisotropic heterogeneous media. They showed that the azimuthal variation of NMO velocity is described by an ellipse in the horizontal plane and is controlled by the spatial derivatives of the ray parameter at the CMP location. Applying their equation to VTI media, they proved that P-wave NMO velocity is fully governed by $V_{P\mathrm{nmo}}(0)$ and η for arbitrary orientations of the CMP line and reflector strike. Hence, for vertical transverse isotropy the parameters V_{P0}, ϵ and δ cannot be resolved individually from P-wave NMO data.

For TI media with a horizontal symmetry axis (HTI), the P-wave kinematic parameters include the azimuth β of the symmetry axis, in addition to V_{P0}, ϵ, and δ. (V_{P0} remains the velocity in the symmetry direction, which is *horizontal* in HTI media, while ϵ and δ are defined with respect to the symmetry axis.) Despite the increase in the number of unknowns, all four moveout parameters can be estimated from azimuthally dependent P-wave NMO velocities measured for a horizontal and dipping reflector (Tsvankin, 1997a; Contreras et al., 1997). Note that moveout inversion in HTI media provides enough information to perform *depth* processing, in contrast to *time* processing in VTI media.

The TI model with a tilted symmetry axis can be considered as intermediate between VTI and HTI. This does not mean, however, that the moveout inversion in TTI media can be understood just by examining the results for the two extreme orientations of the symmetry axis. Indeed, the tilt of the symmetry axis represents an extra parameter to be recovered from moveout data. Tsvankin (1997b) performed an analysis of P-wave NMO velocity in the vertical symmetry plane of TTI media that contains the symmetry axis. To make the problem two-dimensional, he also assumed that the symmetry axis is confined to the dip plane of the reflector. He concluded that the NMO velocity is rather sensitive to the tilt ν and is not fully controlled by η (for fixed ν). Also, Tsvankin's (1997b) results show that the dip dependence of NMO velocity in a single vertical symmetry plane is not sufficient to resolve the medium parameters.

Here, we carry out a 3-D (azimuthal) analysis of normal moveout in TI media with arbitrary tilt and azimuth of the symmetry axis. By employing the 3-D NMO equation of Grechka and Tsvankin (1996), we develop an inversion procedure to obtain all five relevant parameters (V_{P0}, ϵ, δ, β and ν) from P-wave NMO ellipses for two different reflection events. We show that for nonelliptical media and the practically important case of a horizontal and a dipping reflector, the inversion procedure becomes stable if reflector dip reaches at least 30° and the tilt of the symmetry axis exceeds $30-40°$. The generalized Dix differentiation (Tsvankin et al., 1997) allows us to extend the parameter-estimation methodology to vertically heterogeneous TTI media. To estimate the shear-wave velocity V_{S0} in the symmetry direction and increase the overall stability of the inversion procedure, the P-wave NMO velocities for horizontal and dipping events can be supplemented with the SV-wave NMO ellipse from a horizontal reflector.

Basic theory of azimuthally varying NMO velocity

Equation of the NMO ellipse

Here, we give an overview of the analytic representation of NMO velocity in anisotropic media. In conventional acquisition design, the maximum source-receiver offset

is close to the distance between the common midpoint (CMP) and the reflector. For these moderate offsets x, reflection moveout t is usually close to a hyperbola (e.g., Taner and Koehler, 1969; Tsvankin and Thomsen, 1994),

$$t^2(x,\alpha) \approx t_0^2 + \frac{x^2}{V_{\rm nmo}^2(\alpha)}\,, \qquad (3)$$

where t_0 is the two-way zero-offset traveltime and $V_{\rm nmo}(\alpha)$ is the normal-moveout velocity, which generally depends on the azimuth α of the CMP line. As shown by Grechka and Tsvankin (1996), NMO velocity of any pure mode can be expressed as

$$V_{\rm nmo}^{-2}(\alpha) = W_{11}\cos^2\alpha + 2\,W_{12}\sin\alpha\cos\alpha + W_{22}\sin^2\alpha\,, \qquad (4)$$

where $W_{ij} = \tau_0\,\partial p_i/\partial x_j$ $(i,j=1,2)$, $\tau_0 = t_0/2$ is the one-way zero-offset traveltime, p_i are the horizontal components of the slowness vector for one-way rays emanating from the zero-offset reflection point, and x_i are the horizontal spatial coordinates; the derivatives are evaluated at the common midpoint. (For brevity, below we will not show the azimuth α explicitly as an argument of the NMO-velocity function; the value of α in each case will be clear from the context.)

Equation (4) is valid for pure modes in arbitrary anisotropic heterogeneous media as long as the reflection traveltime can be expanded in a Taylor series in x_i near the CMP location. Unless reflection traveltime decreases with offset in a certain direction leading to so-called "reverse moveout" (i.e., there is at least one azimuth α for which $V_{\rm nmo}^2(\alpha) < 0$), the symmetric matrix $\mathbf{W}$ is positive definite, and equation (4) describes an *ellipse*. Clearly, the NMO ellipse is fully determined by the three elements of the matrix $\mathbf{W}$.

Homogeneous arbitrary anisotropic layer

For a homogeneous anisotropic layer above a dipping reflector, the matrix $\mathbf{W}$ can be represented as the following function of the slowness components p_i (Tsvankin et al., 1997):

$$\mathbf{W} = \frac{p_1 q_{,1} + p_2 q_{,2} - q}{q_{,11}q_{,22} - q_{,12}^2} \begin{pmatrix} q_{,22} & -q_{,12} \\ -q_{,12} & q_{,11} \end{pmatrix}\,, \qquad (5)$$

where $q \equiv q(p_1,p_2) \equiv p_3$ denotes the vertical component of the slowness vector, $q_{,i} \equiv \partial q/\partial p_i$, and $q_{,ij} \equiv \partial^2 q/\partial p_i \partial p_j$; the horizontal slowness components p_1 and p_2 and all derivatives are evaluated for the zero-offset ray.

Note that p_1 and p_2 control the reflection slope on the zero-offset (stacked) section and can be obtained directly (unlike reflector dip) from reflection data. The vertical slowness $q = q(p_1,p_2)$ in a known anisotropic model can be found by solving the Christoffel equation for given values of p_1 and p_2. Then, implicit differentiation of Christoffel equation yields the derivatives $q_{,i}$ and $q_{,ij}$ (Tsvankin et al., 1997). Therefore, equation (5) provides a simple and numerically efficient recipe for obtaining NMO velocity of pure modes in a layer with any anisotropic symmetry.

NMO velocity in TTI media: special cases

Normal moveout for steep reflectors

Generation of a specular zero-offset reflection requires that some portion of the incident wavefront be parallel to the reflecting interface or, in other words, that the slowness (or phase-velocity) vector for this segment be orthogonal to the reflector. If the wavefront of the downgoing wave is symmetric with respect to the horizontal plane, specular reflections in a homogeneous layer exist for the whole range of dips from 0° to 90° (Tsvankin, 1997b). Obviously, this condition is always satisfied in models with a horizontal symmetry plane, such as vertical and horizontal transverse isotropy. A tilt of the symmetry axis, however, makes the wavefront asymmetric with respect to horizontal, and its cross-sections in some azimuthal directions may contain only a limited range of phase angles. As illustrated in Figure 1, the phase (wavefront) vector corresponding to a horizontal ray may point down, and the reflection traveltime from the non-vertical interface normal to the phase vector will not change with offset in the ray direction (i.e., the NMO velocity in this direction becomes infinite). Even steeper interfaces reflect all incident rays downward and, therefore, become invisible on surface seismic data. If the medium is heterogeneous and velocity increases with depth, the "missing" dips may produce reflected arrivals at the surface, but these reflections would represent *turning* rays.

Tsvankin (1997b) studied the existence of specular reflections for the "2-D" TTI model with the symmetry axis confined to the dip plane of the reflector. He showed that if the symmetry axis is tilted towards the reflector, the maximum phase (wavefront) angle in the dip plane typically is smaller than 90°, and steeper interfaces do not generate reflected arrivals at the surface. In contrast, for symmetry axis tilted away from the reflector, it is possible to record reflections even from interfaces with dips exceeding 90° (overhang structures) with rays that are not turning.

Here, we treat a more general situation of the symmetry axis making an arbitrary azimuth with the dip plane of the reflector. Figure 2 shows the dependence of the maximum dip that generates a zero-offset reflected ray on the azimuth of the symmetry axis for a particular TTI model. For the maximum dip, the zero-offset ray is *horizontal*, and the NMO velocity in the ray direction is infinite, which means that the NMO ellipse degenerates into two parallel straight lines (Grechka and Tsvankin, 1996). If the symmetry axis is confined to the dip plane

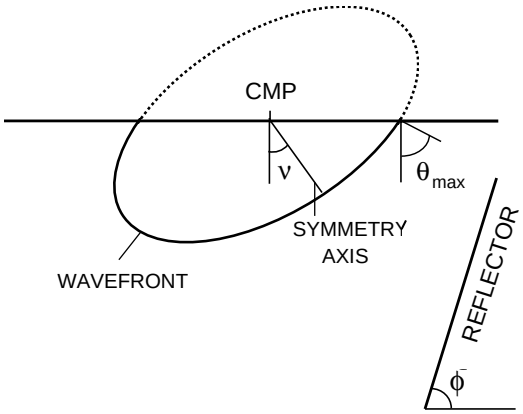

Figure 1. The P-wavefront for a transversely isotropic medium with a symmetry axis tilted towards the reflector. The increase in phase and group velocity away from the symmetry axis in this model reduces the angular range of the wavefront normals in the segment of the wavefront propagating towards the reflector. The maximum phase (wavefront) angle in the right lower quadrant is $\theta_{\max} = \phi < 90^\circ$.

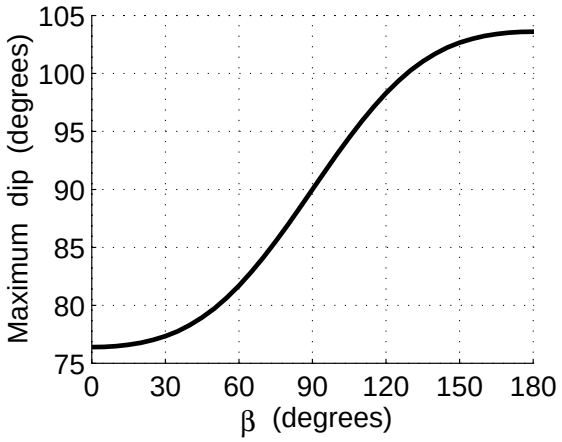

Figure 2. The dip of the steepest reflector that will produce a zero-offset P-wave reflection in a homogeneous TTI layer; β is the azimuth of the symmetry axis with respect to the dip plane of the reflector. The tilt of the symmetry axis $\nu = 25^\circ$, $\epsilon = 0.25$, and $\delta = 0.05$. For $\beta = 0^\circ$, the symmetry axis points *towards* the reflector; for $\beta = 180^\circ$ it is tilted *away* from the reflector.

and points towards the reflector ($\beta = 0$), the maximum dip is just 76° for this model, which agrees with the result of Tsvankin (1997b, Figure 3). As the symmetry axis deviates from the dip plane, the range of "missing" dips becomes more narrow and vanishes altogether for $\beta = 90^\circ$, when the horizontal projection of the symmetry axis coincides with the reflector strike. In this case, the horizontal ray in the dip direction belongs to the isotropy plane and, therefore, is orthogonal to the wavefront. As a result, the segment of the wavefront propagating horizontally in the dip plane should generate a zero-offset reflection from a vertical interface, and the maximum visible dip is indeed equal to 90°. For azimuth β larger than 90°, the maximum dip exceeds 90°, so it is possible to record surface reflections from overhang structures. For the symmetry axis back in the dip plane but, now tilted *away* from the reflector ($\beta = 180^\circ$), the maximum dip reaches 103°.

It should be emphasized that it does not take a large tilt of the symmetry axis for the maximum dip to deviate considerably from 90° (in Figure 2, $\nu = 25^\circ$). As discussed by Tsvankin (1997b), the dependence of the maximum dip on ν is not symmetric with respect to $\nu = 45^\circ$; the most pronounced variations in the maximum dip correspond to tilts well below 45°.

Elliptical anisotropy

A transversely isotropic model with any orientation of the symmetry axis becomes elliptically anisotropic if $\epsilon = \delta$. For elliptical anisotropy, the P-wave slowness surface and wavefront (group-velocity surface) have an ellipsoidal shape, while the SV-wave velocity is equal to V_{S0} in all directions (i.e., is independent of angle). Although the condition $\epsilon = \delta$ is seldom satisfied for subsurface formations (Thomsen, 1986), elliptical models require a special treatment in the inversion procedure and, therefore, have to be considered separately.

Tsvankin (1997b) showed that for elliptical anisotropy the dip-dependence of NMO velocity, expressed through the ray parameter p of the zero-offset ray, is exactly the same as in isotropic media:

$$V_{\rm nmo}(p) = \frac{V_{\rm nmo}(0)}{\sqrt{1 - p^2\, V_{\rm nmo}^2(0)}}\,; \qquad (6)$$

$V_{\rm nmo}(0)$ corresponds to a horizontal reflector. This result, however, is limited to the dip plane of the reflector, under the assumption that this plane contains the symmetry axis of the medium.

Analysis of equation (5) shows that in elliptical media the dependence of the P-wave NMO velocity on p_1 and p_2 remains isotropic for arbitrary orientations of the symmetry axis and reflector normal, and any azimuth of the CMP line. The P-wave phase-velocity function for elliptical anisotropy is given by

$$V_P(\theta) = V_{P0}\sqrt{1 + 2\delta \sin^2\theta}\,, \qquad (7)$$

where θ is the angle between the phase-velocity (slowness) vector and the symmetry axis. Representing θ through the slowness components p_1, p_2 and q and the symmetry-axis orientation (defined by the angles ν and β) yields

$$\cos\theta = V_P\,(p_1 \sin\nu\cos\beta + p_2 \sin\nu\sin\beta + q\cos\nu)\,. \qquad (8)$$

Combining equations (7) and (8) and taking into account that $V_P^2 = (p_1^2 + p_2^2 + q^2)^{-1}$ leads to a quadratic equation for q as a function of p_1 and p_2. Substituting $q(p_1, p_2)$ into equation (5), we find the following equation for the matrix $\mathbf{W}$ in elliptically anisotropic media:

$$W_{ij}(p_1, p_2) = W_{ij}(0, 0) - p_i p_j \,. \tag{9}$$

It is easy to verify that equation (9) is *identical* to the dependence of W_{ij} on p_1 and p_2 for isotropic media. Hence, the influence of elliptical anisotropy on NMO velocity in equation (9) is hidden in the NMO ellipse for horizontal events $[W_{ij}(0, 0)]$. This result has serious implications for the inversion procedure discussed below. Equation (9), as any other isotropic kinematic relationship, can be also used for SV-waves in elliptical media.

The isotropic form of the function $W_{ij}(p_1, p_2)$ also means that conventional dip-moveout algorithms developed for isotropic media are valid for elliptical anisotropy with any orientation of the axes. Since reflection moveout in elliptical media is purely hyperbolic (Uren et al., 1990), all isotropic time-related processing methods (NMO and DMO corrections, prestack and poststack time migration) can be used for elliptical anisotropy without any modification. These conclusions, as well as equation (9), always apply to SH-waves because their propagation is any TI medium is governed by the elliptical dependencies.

TI media with the symmetry axis perpendicular to the reflector

Before considering transversely isotropic media with arbitrary tilt of the symmetry axis, it is useful to discuss the important special case of the symmetry axis orthogonal to a dipping reflector. Such a model is typical for TI formations with the symmetry axis perpendicular to the layering (e.g., shales) that were tilted due to tectonic processes after sedimentation. The simplicity of this model makes it possible to obtain concise *exact* expressions for the NMO ellipse in terms of the medium parameters.

Since the dip plane of the reflector contains the symmetry axis, it becomes a vertical symmetry plane for the whole model and determines the orientation of the NMO ellipse. The semi-axis of the ellipse that lies in the dip plane (the "dip component" of the NMO velocity) is given by (Tsvankin, 1995)

$$V_{\rm nmo}^{(1)}(\phi) = \frac{V_{\rm nmo}(0)}{\cos\phi} \,. \tag{10}$$

Here ϕ is the reflector dip and $V_{\rm nmo}(0)$ is the NMO velocity from a horizontal reflector obtained under the assumption that the symmetry axis remains perpendicular to the reflector (i.e., it is vertical for a horizontal reflector). Equation (10) is identical to the cosine-of-dip dependence of normal-moveout velocity in isotropic media (Levin, 1971), with $V_{\rm nmo}(0)$ replacing the medium velocity.

Introducing the ray parameter $p = \sqrt{p_1^2 + p_2^2}$ into equation (10), we obtain

$$V_{\rm nmo}^{(1)}(p) = \frac{V_{\rm nmo}(0)}{\sqrt{1 - p^2 V_0^2}} \,, \tag{11}$$

where $V_0 = \sin\phi/p$ is the symmetry-direction velocity of the mode under consideration (it may be either a P- or an S-wave). Since in anisotropic media $V_{\rm nmo}(0)$ and V_0 generally are different, equation (11) does not coincide with the corresponding isotropic expression. It is interesting to examine whether the *strike component* of the NMO velocity $V_{\rm nmo}^{(2)}$ provides any additional information about the medium. Straightforward, but tedious, algebraic transformations of equation (5) give

$$V_{\rm nmo}^{(2)} = V_{\rm nmo}(0) \,. \tag{12}$$

For P-waves this result can be more easily obtained in the weak-anisotropy approximation (discussed in detail below) by substituting the relation $\tan\nu = \tan\phi = p_1/p_3$ into equation (A7) for W_{22}. Therefore, $V_{\rm nmo}^{(2)}$ is simply equal to the zero-dip NMO velocity and is completely independent of dip, comparable to the result of Levin (1971) for isotropic media.

Combining the two semi-axes of the NMO ellipse [equations (11) and (12)] and obtaining p from the zero-offset section, we can find $V_{\rm nmo}(0)$ and the symmetry-direction velocity V_0 (if the dip is not too mild). Since for the P-wave $V_{P\rm nmo}(0) = V_{P0}\sqrt{1 + 2\delta}$ [equation (1)], the P-wave NMO ellipse for a dipping event yields the anisotropic parameter δ in addition to the symmetry-direction velocity V_{P0}. [Likewise, the NMO ellipse of the SV-wave provides the symmetry-direction velocity V_{S0} and the anisotropic parameter $\sigma = (V_{P0}^2/V_{S0}^2)(\epsilon - \delta)$.]

Both parameters can be determined even from 2-D data acquired in the dip plane if the zero-dip velocity $V_{P\rm nmo}(0)$ was recovered from a horizontal event. Note that for the NMO velocity from a horizontal reflector to be equal to $V_{\rm nmo}(0)$ in equation (11), the symmetry axis for the horizontal event should be vertical. We can imagine, for instance, that the reflecting interface may have a gradually changing slope with the symmetry axis remaining orthogonal to the reflector. In the inversion procedure described below, however, we fix the orientation of the symmetry axis and use the NMO ellipses for horizontal and dipping events to obtain the medium parameters.

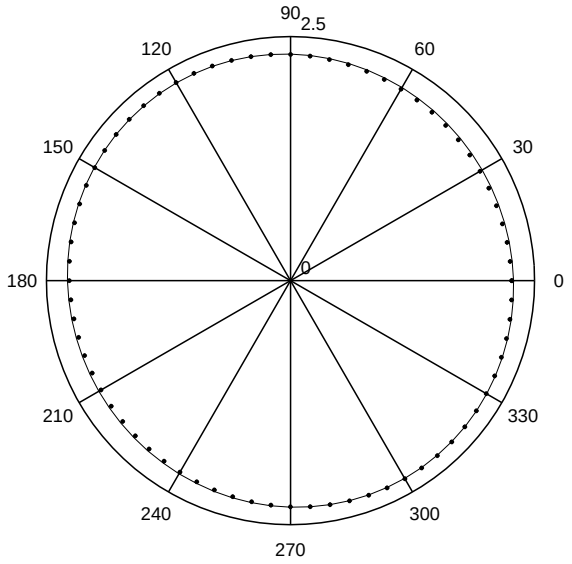

Figure 3. Quasi-circular P-wave NMO ellipses in a horizontal TTI layer. Solid – the ellipse computed using equation (5); dotted – the ellipse reconstructed using the hyperbolic equation (3) from ray-traced traveltimes computed along four CMP lines at azimuths 0°, 45°, 90°, and 135° (the azimuth is shown around the plot); the spreadlength is equal to the thickness of the layer. The relevant medium parameters are $V_{P0} = 2.0$ km/s, $\epsilon = 0.2$, $\delta = 0.1$, $\beta = 30°$, and $\nu = 45°$.

P-wave NMO ellipse in weakly anisotropic TTI media

Horizontal layer

Although equations (4) and (5) give a concise representation of azimuthally-varying NMO velocity, the dependence of $V_{\rm nmo}$ on the model parameters is hidden in the components of the slowness vector. To understand the influence of the axis orientation and anisotropic parameters on the P-wave normal moveout, we linearize equation (5) with respect to ϵ and δ assuming that $|\epsilon| \ll 1$ and $|\delta| \ll 1$ (Appendix A). The final expressions (A7) and (A8) correspond to the coordinate system in which the azimuth of the symmetry axis $\beta = 0$ (i.e., the symmetry axis is in the $[x_1, x_3]$-plane, see Figure A1). Note that the shear-wave velocity V_{S0} in the symmetry direction does not appear in the linearized NMO equations because all P-wave kinematic signatures in the weak-anisotropy approximation are independent of V_{S0} (Tsvankin, 1996).

For a horizontal reflector ($p_1 = p_2 = 0$) equations (A7) and (A8) can be simplified to

$$W_{11} = \frac{1}{V_{P0}^2}\left[1 - 2\delta + 2\epsilon\sin^2\nu - 14\,(\epsilon-\delta)\sin^2\nu\cos^2\nu\right], \qquad (13)$$

$$W_{12} = 0\,, \qquad (14)$$

$$W_{22} = \frac{1}{V_{P0}^2}\left[1 - 2\delta - 2\,(\epsilon-\delta)\sin^2\nu\,(1+\cos^2\nu)\right]. \qquad (15)$$

Since $W_{12} = 0$, the semi-axes of the P-wave NMO ellipse for a horizontal reflector are parallel to the coordinate axes x_1 and x_2. This result could be expected because the $[x_1, x_3]$-plane contains the symmetry axis and, therefore, represents a symmetry plane of the horizontal TTI layer. In the case of vanishing W_{12}, the quantities W_{11} and W_{22} are reciprocal to the squared NMO velocities along the semi-axes of the ellipse (Grechka and Tsvankin, 1996):

$$W_{ii} = \frac{1}{[V_{P\rm nmo}^{(i)}(0)]^2}\,, \qquad (i = 1, 2)\,. \qquad (16)$$

The velocity $V_{P\rm nmo}^{(1)}(0)$ defined by equations (13) and (16) corresponds to the CMP line in the vertical plane that contains the symmetry axis. Equations (13) and (16) are equivalent to the result of Tsvankin (1997b) [his equation (23)] who studied normal moveout only in this vertical symmetry plane. The second semi-axis of the NMO ellipse, $V_{P\rm nmo}^{(2)}(0)$ [equations (15) and (16)], is generally different from $V_{P\rm nmo}^{(1)}(0)$. Therefore, equations (13) – (15) provide us with three constraints for the layer parameters: the orientation of the NMO ellipse depends on the azimuth β of the symmetry axis, while the values of the semi-axes give two more equations for all five parameters. Note that the azimuth of the symmetry axis cannot be unambiguously found from the NMO ellipse from a horizontal reflector, because β can be equal to the azimuth of either semi-major or semi-minor axis depending on the medium parameters. For horizontal transverse isotropy ($\nu = 0$) due to parallel penny-shaped cracks, the symmetry axis typically coincides with the semi-major axis of the P-wave NMO ellipse (Tsvankin, 1997a).

The number of equations, however, reduces to two if the NMO ellipse degenerates into a circle, i.e.,

$$V_{P\rm nmo}^{(1)}(0) = V_{P\rm nmo}^{(2)}(0)\,. \qquad (17)$$

Obviously, for VTI media ($\nu = 0$) NMO velocity is always independent of azimuth, and $V_{P\rm nmo}^{(1)}(0) = V_{P\rm nmo}^{(2)}(0) = V_{P\rm nmo}(0) = V_{P0}\sqrt{1+2\delta}$ [equation (1)]. It is interesting that condition (17) can also be satisfied for *azimuthally anisotropic* media with a tilted symmetry axis. Substituting equations (13), (15), and (16) into equation (17) and assuming $\nu \neq 0$, we find

$$2\epsilon - \delta - 6\,(\epsilon-\delta)\cos^2\nu = 0\,. \qquad (18)$$

For instance, if the symmetry axis is horizontal ($\cos\nu = 0$), relation (18) gives

$$2\epsilon - \delta = 0\,, \qquad (19)$$

which represents a known condition for the P-wave NMO ellipse in weakly anisotropic HTI media to degenerate into a circle. The ellipticity of P-wave NMO velocity in HTI media is governed by the coefficient $\delta^{(V)} \approx 2\epsilon - \delta$ (Tsvankin, 1997a), which goes to zero if equation (19) is satisfied.

An example of azimuthally-independent NMO-velocity for TI media with an intermediate tilt angle of 45° is shown in Figure 3. Equation (18) with $\nu = 45^\circ$ yields $\epsilon - 2\delta = 0$, so for the model from Figure 3 the semi-axes of the NMO ellipse should be equal to each other. Although equation (18) is an approximation valid only for weakly anisotropic media, the exact NMO ellipse calculated using equation (5) is, indeed, almost circular.

Another important point illustrated by Figure 3 is that the theoretical NMO ellipse (solid) is close to the ellipse reconstructed from ray-traced traveltimes for spreadlength equal to the reflector depth (dotted). The difference between the two ellipses, caused by the deviation of the moveout curve from the analytic hyperbola, is limited by 1.1%. Clearly, the influence of nonhyperbolic moveout on P-wave moveout velocity can be ignored, as long as the maximum offset does not exceed reflector depth. The same conclusion was drawn by Tsvankin (1997b) in his study of the 2-D moveout problem in TTI media.

Dipping TTI layer

The P-wave NMO ellipse from a horizontal reflector provides either two or three constraints on the parameters of the TTI layer, depending on whether or not the ellipse degenerates into a circle. To resolve all five relevant layer parameters (V_{P0}, ϵ, δ, β, and ν), we suggest also including the NMO ellipse from a dipping reflector (i.e., three more equations) in the inversion procedure.

Although there seems to be enough equations to recover all unknowns, in certain situations the parameters cannot be resolved individually. The weak-anisotropy approximation of the P-wave NMO ellipse [equations (A7) and (A8)] helps to identify the trade-offs between model parameters and study the stability of the inversion procedure. For instance, equation (A7) shows that the anisotropic coefficients in all dip-dependent terms appear only as the *difference* $\epsilon - \delta$. Still, ϵ and δ can be resolved individually using the NMO ellipse for horizontal events [equations (13) and (15)], unless the tilt is relatively small. For mild tilts ν the medium approaches VTI, and the NMO velocity from a horizontal reflector yields a single quantity ($V_{P0}\sqrt{1+2\delta}$), while the dip dependence of NMO velocity is controlled by $\eta \approx \epsilon - \delta$ (Alkhalifah and Tsvankin, 1995). Thus, ϵ and δ can be estimated separately, but only for a sufficiently large tilt of the symmetry axis.

A similar constraint applies to the reflector dip, which should not be too mild for the dip-dependence of NMO velocity to be sensitive enough to the anisotropic parameters. [The anisotropic dip terms $\hat{W}_{ij}$ in the weak-anisotropy approximation (A8) can be used to make appropriate estimates.] On the whole, determination of the five relevant parameters of TTI media from the P-wave NMO ellipses for a horizontal and a dipping reflector should be feasible if both the reflector dip and the tilt of the symmetry axis are not "too small." In the next section, we quantify this statement by performing the actual inversion based on the exact NMO equation.

Parameter estimation in a TTI layer using P waves

Here, we present results of the numerical inversion of P-wave NMO velocity for a single homogeneous TTI layer. The NMO ellipses for a horizontal ($\tilde{\mathbf{W}}^{P\mathrm{hor}}$) and a dipping ($\tilde{\mathbf{W}}^{P\mathrm{dip}}$) event are inverted for five medium parameters – the velocity V_{P0} in the symmetry direction, Thomsen's anisotropic coefficients ϵ and δ, the tilt ν and the azimuth β of the symmetry axis. The parameters are found by minimizing the least-squares objective function

$$\mathcal{F}_P = \sum_{i,j=1}^{2} w_h \left(W_{ij}^{P\mathrm{hor}} - \tilde{W}_{ij}^{P\mathrm{hor}}\right)^2 + w_d \left(W_{ij}^{P\mathrm{dip}} - \tilde{W}_{ij}^{P\mathrm{dip}}\right)^2 , \qquad (20)$$

where the matrices $\mathbf{W}^{P\mathrm{hor}}$ and $\mathbf{W}^{P\mathrm{dip}}$ are calculated using the exact equation (5) for a particular set of parameters. The weights

$$w_h = 4\,(\tilde{W}_{11}^{P\mathrm{hor}} + \tilde{W}_{22}^{P\mathrm{hor}})^{-2} \qquad (21)$$

and

$$w_d = 4\,(\tilde{W}_{11}^{P\mathrm{dip}} + \tilde{W}_{22}^{P\mathrm{dip}})^{-2} \qquad (22)$$

are used to equalize the contributions of the two ellipses in equation (20). The minimization of the objective function was carried out using the simplex method. Although in principle the nonlinear system (20) might have multiple solutions, extensive numerical testing shows that for error-free input data and a realistic starting model (i.e., $|\epsilon| < 1$, $|\delta| < 1$) the inversion algorithm always converges towards the correct set of parameters.

For numerical testing, we computed the matrices $\tilde{\mathbf{W}}^{P\mathrm{hor}}$ and $\tilde{\mathbf{W}}^{P\mathrm{dip}}$ from equation (5) and added Gaussian noise with a variance of 2% to simulate errors in velocity picking. Figure 4 shows the results of parameter estimation for TTI layers with different tilts ν of the symmetry axis. Each dot on the plots corresponds to the inversion result for a particular realization of random errors in the NMO ellipses; the inversion procedure

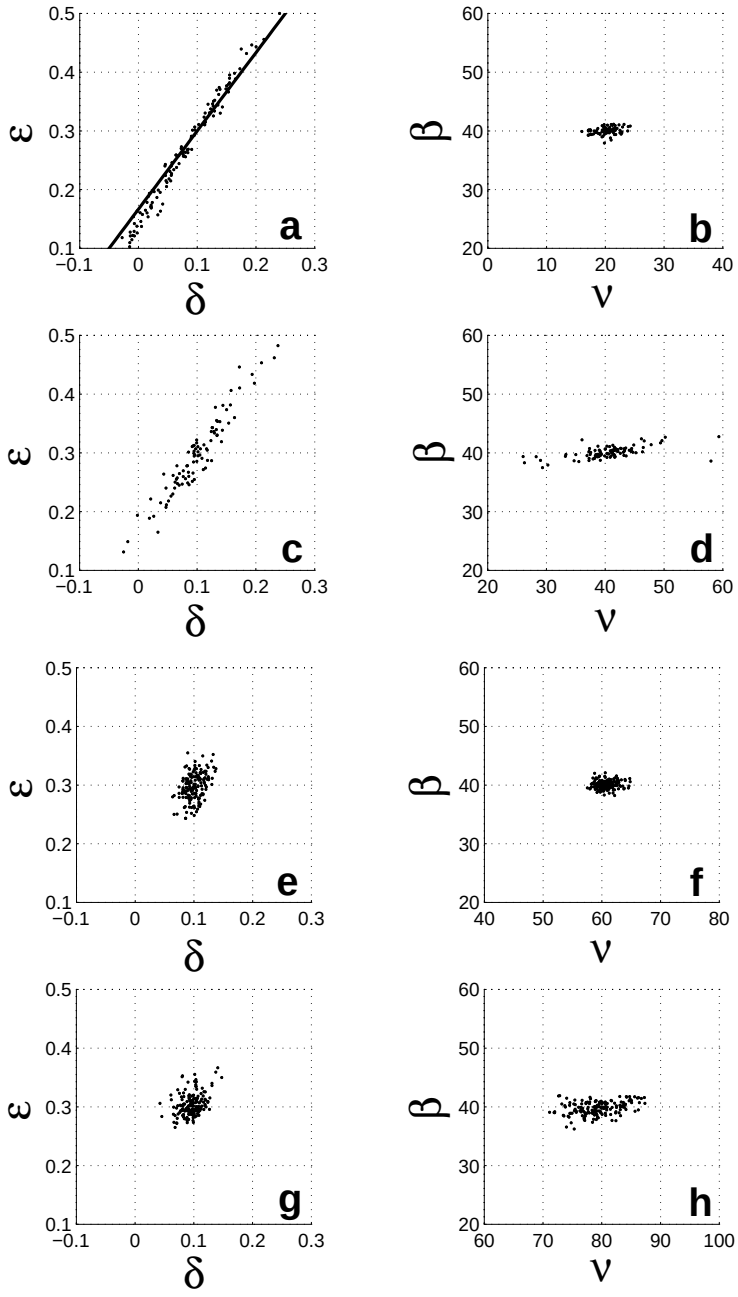

Figure 4. Inverted values of the parameters ϵ, δ, β, and ν in a homogeneous TTI layer. As the input data we use the P-wave NMO ellipses from a horizontal and a dipping reflector (the dip $\phi = 60°$, the azimuth $= 50°$). Both ellipses were distorted by random noise with a variance of 2%. The actual values are: $V_{P0} = 2.0$ km/s, $V_{S0} = 1.2$ km/s, $\epsilon = 0.3$, $\delta = 0.1$, $\beta = 40°$; the tilt ν is equal to 20° in (a) and (b), 40° in (c) and (d), 60° in (e) and (f), and 80° in (g) and (h). The solid line on plot (a) indicates ϵ's and δ's corresponding to the correct value of $\eta = 0.167$.

for each model was repeated 200 times. The mean values of all parameters were recovered accurately despite the fact that we used an *incorrect* shear-wave velocity $V_{S0} = V_{P0}/2$ to perform the inversion. Hence, in agreement with the results of Tsvankin (1996, 1997b) and the weak-anisotropy approximations (A7) and (A8), V_{S0} has a negligible influence on P-wave moveout in TI media.

Figure 4 also confirms the conclusion of the previ-

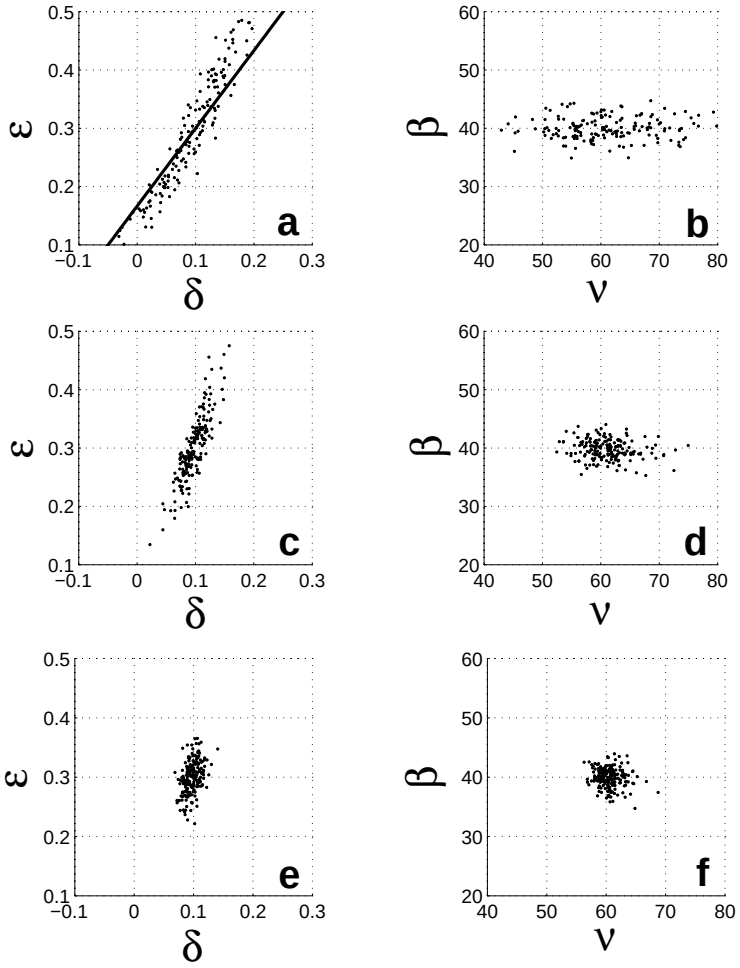

Figure 5. Same as Figure 4, but for variable reflector dip. The parameters V_{P0}, ϵ, δ, β and the reflector azimuth are the same as those in Figure 4; the tilt of the symmetry axis $\nu = 60°$. The reflector dip ϕ is equal to 20° in (a) and (b), 30° in (c) and (d), and 40° in (e) and (f). The solid line on plot (a) corresponds to the correct value of $\eta = 0.167$.

ous section that the inversion becomes more stable with increasing tilt of the symmetry axis. While the inverted values of ϵ and δ are close to the correct ones for the tilts $\nu = 60°$ and $\nu = 80°$ (the variance ϵ and δ in Figures 4e and 4g is less than 0.02), the deviations visibly increase for $\nu = 40°$ (Figure 4c) and, especially, for $\nu = 20°$ (Figure 4a). The inversion results for $\nu < 30 - 40°$ are so sensitive to errors in the input parameters that P-wave NMO velocity cannot be used to resolve ϵ and δ individually. Nonetheless, the inverted values of ϵ and δ are tightly clustered near the line corresponding to the correct value of η [see equation (2)]. Therefore, η is the only combination of the anisotropic parameters constrained by the P-wave NMO velocity for mild tilts ν, which agrees with the known result of Alkhalifah and Tsvankin (1995) for vertical transverse isotropy.

The accuracy in the P-wave velocity V_{P0} in the symmetry direction (not shown in Figure 4) exhibits a similar dependence on the tilt, with the scatter in the inversion results monotonically increasing with decreasing ν. The variance in V_{P0} changes from a small value of 0.01 km/s (0.5% of the correct V_{P0}) for a near-horizontal symmetry axis ($\nu = 80°$) to 0.23 km/s (11.5%) for a tilt of 20°. For a near-vertical symmetry axis, P-wave normal moveout can be used to obtain the zero-dip NMO velocity ($V_{P0}\sqrt{1+2\delta}$), but not V_{P0} or δ separately (see the analysis for VTI media in Alkhalifah and Tsvankin, 1995).

Another interesting observation, this time from the right-column plots in Figure 4, is that the azimuth β of the symmetry axis is well-constrained for all four tilts ν, while the variance in the tilt itself is more significant.

Overall, the accuracy in both β and ν is quite satisfactory for a wide range of tilts; the only exception is "quasi-VTI" models with small $\nu < 10^\circ$ (not shown here) for which the orientation of the symmetry axis does not have much influence on normal moveout.

The inversion results in Figure 4 were obtained for a rather favorable (large) reflector dip $\phi = 60^\circ$. As expected, the inversion becomes less stable as the dipping reflector tilts toward horizontal (Figure 5). Each row of plots in Figure 5 should be compared with Figures 4e,f, which were generated for the same $\nu = 60^\circ$. While the scatter in the inverted parameters for the dips $\phi = 40^\circ$ (Figures 5e,f) and $\phi = 60^\circ$ (Figures 4e,f) is comparable, the results deteriorate for a smaller $\phi = 30^\circ$ (Figures 5c,d) and become quite unstable for $\phi = 20^\circ$ (Figures 5a,b). The inverted values of ϵ and δ in Figure 5a still cluster around a straight line, but this line is no longer described by the actual parameter η. It is interesting that the scatter in the parameters responsible for the symmetry-axis orientation is much more sensitive to the reflector dip (the right column of plots in Figure 5) than to the tilt of the axis (Figure 4). The variance in the symmetry-direction velocity V_{P0} (not shown) also increases from 1.4% for $\phi = 40^\circ$ to 2.8% for $\phi = 30^\circ$ to more than 7% for $\phi = 20^\circ$.

Therefore, the dip should reach at least 30° for the inversion to be reasonably stable. Similar values of the minimum dip were given by Alkhalifah and Tsvankin (1995), who used the dip dependence of NMO velocity in the inversion for the anisotropic parameter η in VTI media. On the other hand, the reflector should not be too steep, because, for dips approaching 90°, specular reflections and the NMO ellipse may not exist at all (see the discussion above).

We conclude that the moveout inversion based on the P-wave NMO ellipses for a horizontal and a dipping reflector yields sufficiently stable results if both the reflector dip and tilt of the axis exceed $30 - 40^\circ$.

In addition to the constraints on ν and ϕ, stable moveout inversion requires that the parameters ϵ and δ be sufficiently different from one another. If $\epsilon = \delta$ (the medium is elliptical), the dip dependence of the P-wave NMO velocity is purely isotropic [equation (9)], and the only information contained in the NMO ellipse for the dipping event is that $\epsilon = \delta$. This implies that a single P-wave NMO ellipse for a horizontal event (three equations) has to be used to recover the four remaining parameters (V_{P0}, ϵ, ν, and β). Obviously, this inversion is ambiguous, and it is possible to find a family of elliptical models with identical NMO ellipses from horizontal and dipping reflectors (Figure 6). The inversion becomes feasible only if one of the parameters is known a priori.

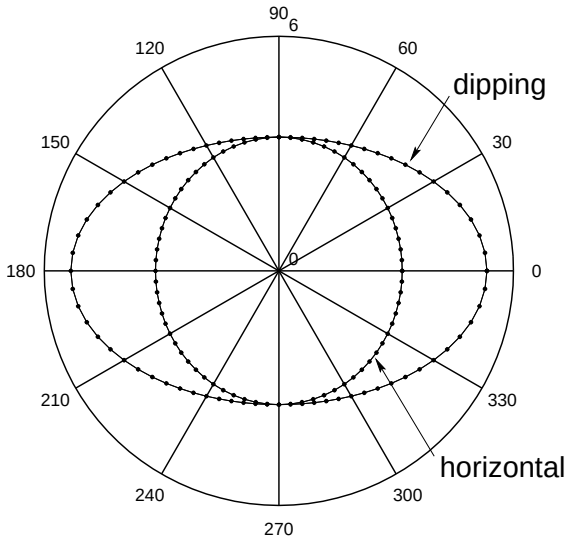

Figure 6. P-wave NMO ellipses for horizontal and dipping reflectors calculated from the exact equation (5) in an elliptical TTI layer for two different sets of medium parameters. The solid ellipses are computed for $V_{P0} = 3.0$ km/s, $\epsilon = \delta = 0.15$, $\nu = 50^\circ$; for the dipping reflector, $\phi = 50^\circ$. For the dotted ellipses, $V_{P0} = 2.443$ km/s, $\epsilon = \delta = 0.4806$, $\nu = 25.34^\circ$, $\phi = 39.98^\circ$. The azimuth of the symmetry axis and that of the dipping reflector are equal to zero for both models; the horizontal slowness of the zero-offset ray for the dipping event is $p_1 = 0.255$.

For instance, if the symmetry axis is assumed to be horizontal and $\nu = 90^\circ$ (HTI media), the remaining three parameters can be obtained from the NMO ellipse from a horizontal reflector. Below, we show that the parameters of elliptical media can be resolved for arbitrary orientation of the symmetry axis if P-wave moveout data are supplemented with the SV-wave NMO ellipse from a horizontal reflector.

Joint inversion of P- and SV-wave moveout in a TTI layer

P- and SV-wave propagation in transversely isotropic media is controlled by the same set of the stiffness coefficients C_{ij}. If the stiffnesses are replaced with Thomsen parameters, P-wave kinematics becomes independent of the shear-wave symmetry-direction velocity V_{S0}, but both P- and SV-wave velocities are still influenced by V_{P0}, ϵ, δ, and the orientation of the symmetry axis. Hence, we can expect to increase the stability of the inversion procedure discussed in the previous section by combining P-wave data with SV-wave NMO ellipses.

In this section, we modify our parameter-estimation algorithm by adding the NMO velocity of SV-waves from a horizontal reflector to the input data. The SV-wave NMO ellipse for horizontal events in the weak-anisotropy

approximation can be obtained from the corresponding P-wave equations (13)–(15) by making the following parameter substitutions (Tsvankin, 1995, 1997b): the velocity V_{P0} should be replaced with V_{S0}, ϵ set to zero, and δ replaced with the parameter σ defined as

$$\sigma = \left(\frac{V_{P0}}{V_{S0}}\right)^2 (\epsilon - \delta). \tag{23}$$

This yields the following expressions for the semi-axes of the SV-wave ellipse from a horizontal reflector (the axis x_1 is parallel to the horizontal projection of the symmetry axis):

$$V^{(1)}_{SV\,\mathrm{nmo}}(0) = V_{S0}\sqrt{1 + 2\sigma\,(1 - 7\sin^2\nu\cos^2\nu)} \tag{24}$$

and

$$V^{(2)}_{SV\,\mathrm{nmo}}(0) = V_{S0}\sqrt{1 + 2\sigma\,\cos^4\nu}, \tag{25}$$

For vertical transverse isotropy ($\nu = 0$), equations (24) and (25) reduce to the azimuthally-independent SV-wave NMO velocity given by Thomsen (1986),

$$V_{SV\,\mathrm{nmo}}(0) = V_{S0}\sqrt{1 + 2\sigma}. \tag{26}$$

The SV-wave NMO ellipse degenerates into a circle not only for VTI media, but also if the above trigonometric functions multiplied with 2σ are identical, i.e., $\cos^2\nu = \frac{1}{6}$ ($\nu = 65.9^\circ$). It is interesting that for a tilt of 65.9° the P-wave NMO ellipse can also become a circle, but only for $\epsilon = 0$ [see equation (18)].

The NMO velocities of P- and SV-waves in a horizontal VTI layer are insufficient for the determination of the vertical velocities and anisotropic coefficients (Tsvankin and Thomsen, 1995). Although the vertical-velocity ratio V_{P0}/V_{S0} can be found from the zero-offset traveltimes, the two NMO velocities still contain three unknown parameters (V_{P0}, δ, and σ or ϵ). The only exception is elliptical anisotropy, for which the SV-wave NMO velocity is independent of angle, and the NMO velocity is simply equal to V_{S0}. Then V_{P0} can be found from the zero-offset traveltimes, and the P-wave NMO velocity yields the anisotropic parameter $\epsilon = \delta$. This inversion procedure, however, is based on the *assumption* that the medium is elliptical, which cannot be verified from the data, unless dipping events or SH data are available.

It seems, however, that for a *tilted* symmetry axis it might be possible to resolve all medium parameters in a horizontal layer even for nonelliptical anisotropy, because we can take advantage of the azimuthal dependence of normal moveout. Indeed, the NMO ellipses of P- and SV-waves in a horizontal TTI layer provide six equations for the medium parameters. Only five of these equations, however, are independent because the two ellipses have the same orientation determined by the azimuth of the symmetry axis. In principle, the number of equations can go down to four if both ellipses degenerate into circles, but the above analysis shows that this situation is highly unlikely*. Including SV-waves also allows us to obtain the ratio of the zero-offset traveltimes $r = t_{P0}/t_{SV0}$ and add a sixth equation into the inversion procedure.

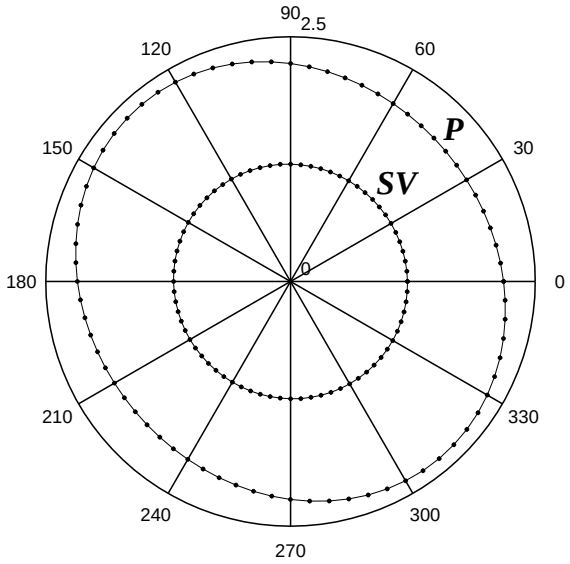

Figure 7. NMO ellipses of P- and SV-waves calculated from equation (5) in a horizontal TTI layer for two different sets of medium parameters. The parameters used to compute the solid ellipses are: $V_{P0} = 2.0$ km/s, $V_{S0} = 1.2$ km/s, $\epsilon = 0.2$, $\delta = 0.1$, $\nu = 60^\circ$. For the dotted ellipses, $V_{P0} = 1.902$ km/s, $V_{S0} = 1.204$ km/s, $\epsilon = 0.273$, $\delta = 0.253$, $\nu = 49.7^\circ$. The azimuth of the symmetry axis $\beta = 40^\circ$ is the same for both models.

Thus, combining P- and SV-data in a horizontal TTI layer results in a system of six nonlinear equations for six unknowns (V_{P0}, V_{S0}, ϵ, δ, ν, and β). Unfortunately, numerical analysis of this system shows that it does not have a unique solution. As illustrated by Figure 7, it is possible to find at least two different realistic TTI models which yield practically identical NMO ellipses of P- and SV-waves. Also, the ratio of the zero-offset traveltimes for both models from Figure 7 is the same ($r = 0.546$).

Since the P- and SV-wave NMO ellipses from a horizontal reflector do not provide enough information for unambiguous parameter estimation, we add the P-wave NMO velocity for a dipping event to the input data and construct the following objective function [compare with

* For weak anisotropy, both ellipses become circles only if the conditions $\cos^2\nu = 1/6$ and $\epsilon = 0$ are satisfied simultaneously.

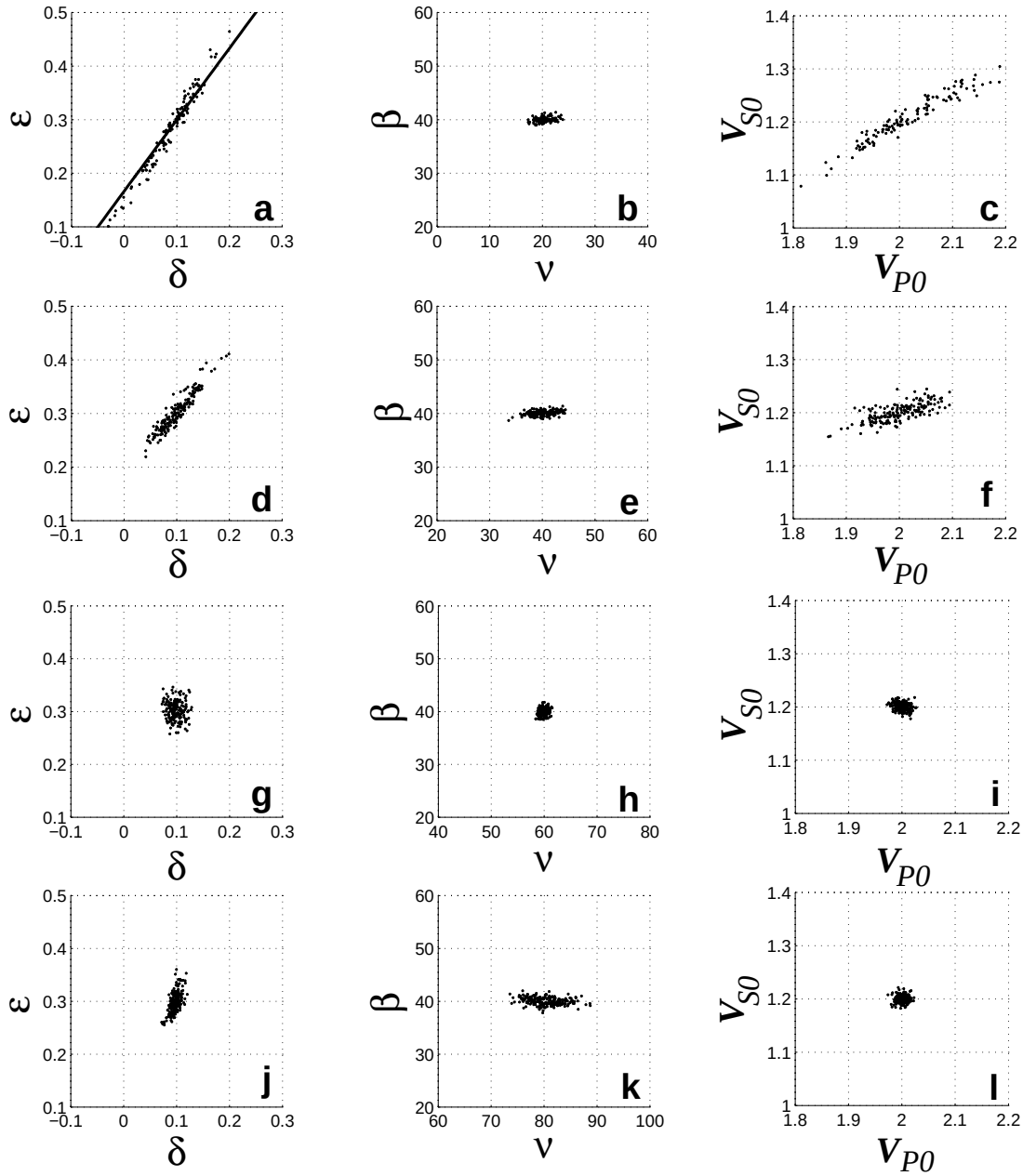

Figure 8. Inverted values of the parameters ϵ, δ, β, ν, V_{P0}, and V_{S0} in a homogeneous TTI layer. For input data, we use the P-wave NMO ellipses from a horizontal and a dipping

equation (20)]:

$$\begin{aligned}\mathcal{F}_{P,SV} &= \left(\frac{r}{\tilde{r}}-1\right)^2 \\ &+ \sum_{i,j=1}^{2} w_h \left(W_{ij}^{P\mathrm{hor}} - \tilde{W}_{ij}^{P\mathrm{hor}}\right)^2 \\ &\quad + w_d \left(W_{ij}^{P\mathrm{dip}} - \tilde{W}_{ij}^{P\mathrm{dip}}\right)^2 \\ &\quad + w_s \left(W_{ij}^{SV\mathrm{hor}} - \tilde{W}_{ij}^{SV\mathrm{hor}}\right)^2 . \end{aligned} \tag{27}$$

As before, $\tilde{\mathbf{W}}$ denote the ellipses measured from the data, while $\mathbf{W}$ are calculated from the exact NMO equation (5). The weighting coefficients w_h and w_d are defined in equations (21) and (22), and w_s is the weight for SV-wave NMO ellipse given by

$w_s = 4\,(\tilde{W}_{11}^{SV\mathrm{hor}} + W_{22}^{SV\mathrm{hor}})^{-2}$.

Compared to the pure P-wave inversion in the previous section, the objective function contains four more equations and only one additional unknown parameter (V_{S0}), so the inversion procedure should become more stable. Overall, the joint inversion of P and SV data involves solving nine nonlinear equations (provided that none of the ellipses degenerates into a circle) for six unknowns – V_{P0}, V_{S0}, ϵ, δ, ν, and β.

Typical results of parameter estimation for a TTI layer obtained by minimizing the objective function (27) are presented in Figure 8. As before, we added Gaussian noise with a variance of 2% to all NMO ellipses and performed the inversion 200 times for different realizations of the input data. Figure 8 exhibits the same general trend as that for the P-wave results in Figure 4: the inversion procedure becomes more stable with increasing tilt ν of the symmetry axis. Comparison of the corresponding plots in Figures 4 and 8 shows, however, that the scatter in the inverted values is higher for the pure P-wave inversion (Figure 4), especially for a tilt of 40°. Therefore, as expected, the addition of the SV-wave NMO ellipse from a horizontal reflector to P-wave data increases the stability of parameter estimation.

Nonetheless, even the combination of P and SV data is not sufficient for resolving all medium parameters in a stable fashion if the tilt of the symmetry axis is small (Figure 8a – 8c). It seems that in the limit of $\nu = 0$ (VTI media) we should be able to find ϵ, δ and the symmetry-direction (vertical) velocities separately because, after obtaining $\eta \approx \epsilon - \delta$ from the dip-dependence of P-wave NMO velocity and the V_{P0}/V_{S0} ratio from the vertical traveltimes, we can determine V_{S0} (and then all other parameters) using the SV-wave velocity for a horizontal event [equation (26)]. However, while this inversion works well on noise-free data, small errors in η propagate with significant amplification into the value of σ [equation (23)] and the vertical velocities. Hence, despite the parameter η being well-resolved (Figure 8a), we observe an increased scatter in V_{P0}, V_{S0}, ϵ and δ for mild tilt angles.

The addition of the SV-wave NMO ellipse for a horizontal reflector does help, however, to overcome the ambiguity of P-wave inversion for elliptical anisotropy. In this case, the dip dependence of the P-wave NMO ellipse is sufficient only to establish the fact that $\epsilon = \delta$, and the parameters V_{P0}, ϵ, ν, and β cannot be found from a single P-wave NMO ellipse for a horizontal event (see the discussion above). The SV-wave phase velocity in elliptical media is independent of angle, so the NMO velocity from a horizontal reflector is simply equal to V_{S0} in any direction. After obtaining V_{S0} from the SV-wave moveout, we can use the ratio of the zero-offset P and SV traveltimes as one more equation for V_{P0}, ϵ, ν, and β, which allows us to resolve all medium parameters. Our numerical analysis shows that this inversion procedure is reasonably stable.

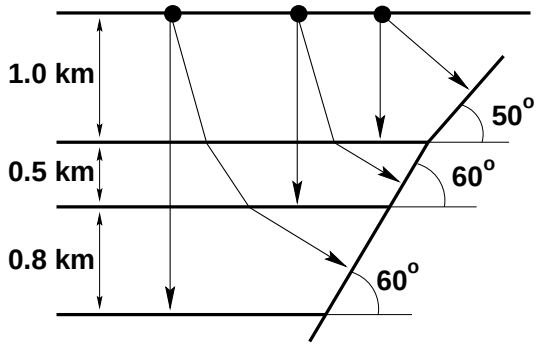

Figure 9. 2-D sketch of the layered TTI model used to test the inversion algorithm. The azimuth of the reflector is 0°; layer thicknesses and reflector dips ϕ in each interval are shown on the plot. Layer parameters are given in Table 1.

Parameter estimation for vertically heterogeneous TTI media

The above discussion was limited to moveout inversion for a single homogeneous TI layer with a tilted symmetry axis. Here, we extend the parameter-estimation methodology to vertically-heterogeneous TTI media composed of a stack of horizontal TTI layers (the orientation of the symmetry axis may be arbitrary) above a dipping reflector. Azimuthally varying NMO velocity for this model can be expressed through the interval NMO ellipses using the generalized Dix equation of Tsvankin et al. (1997). The interval NMO ellipse $\mathbf{W}_\ell$ in layer ℓ can be found by means of the Dix-type differentiation:

$$\mathbf{W}_\ell^{-1} = \frac{\tau(\ell)\mathbf{W}^{-1}(\ell) - \tau(\ell-1)\mathbf{W}^{-1}(\ell-1)}{\tau(\ell) - \tau(\ell-1)}\,, \qquad (28)$$

where $\mathbf{W}(\ell-1)$ and $\mathbf{W}(\ell)$ describe the NMO ellipses for the reflections from the top and bottom of the layer, and $\tau(\ell-1)$ and $\tau(\ell)$ are the corresponding zero-offset traveltimes. Although this equation looks similar to the well-known Dix (1955) formula [one may think about formally replacing the matrices $\mathbf{W}^{-1}$ by the squared NMO velocities], it is much more general because it fully accounts for the simultaneous influence of arbitrary anisotropy and reflector dip on the azimuthally dependent NMO velocity. Equation (28) is not limited to any particular anisotropic symmetry and can be used for all pure reflected modes (P-waves or S-waves). For example, Grechka and Tsvankin (1997) applied this equation to parameter estimation in vertically-heterogeneous orthorhombic media.

Here, we use the generalized Dix equation to invert

Layer	V_{P0} (km/s)	V_{S0} (km/s)	ϵ	δ	ν	β
1	2.00	1.20	0.15	0.10	50.0	20.0
2	2.50	1.60	0.20	0.10	60.0	40.0
3	3.00	1.80	0.30	0.15	40.0	60.0

Table 1. Actual values of the interval parameters for the model in Figure 9. Tilt of the symmetry axis ν and azimuth β are in degrees.

Layer	V_{P0} (km/s)	ϵ	δ	ν	β
1	2.02	0.14	0.09	53.6	19.6
2	2.52	0.19	0.10	60.1	38.9
3	2.91	0.38	0.14	43.7	64.5

Table 2. Inverted interval parameters for the model from Figure 9. The maximum source-receiver offset used in estimating moveout velocities is equal to the distance between the CMP and the corresponding reflector. Compare with the actual values from Table 1.

the reflection traveltimes from horizontal and dipping reflectors for the interval parameters of layered TTI media. The effective and interval NMO ellipses in equation (28) are evaluated for the slowness components of the *zero-offset* ray. In the case of horizontal events, the zero-offset slowness vector is vertical for all reflections (i.e., its horizontal components vanish), and the interval ellipse can be found directly from the effective ellipses for the reflections from the top and bottom of the layer. For dipping reflectors, however, the ray parameters of the zero-offset ray change from layer to layer depending on the reflector dip in a particular layer. Therefore, after carrying out the inversion in the subsurface layer using the technique described in the previous sections, we need to calculate the matrix $\mathbf{W}$ in this layer for the slowness components of the zero-offset reflection from the dipping interface in the *second* layer. Then we obtain the interval NMO ellipse for the dipping event in the second layer from equation (28), combine it with the corresponding ellipse from the horizontal reflector, carry out the inversion in the second layer and continue the layer-stripping procedure downward.

We applied our inversion algorithm to synthetic data generated for a three-layer TTI model with a dipping reflector (e.g., a fault plane) shown in Figure 9. Note that the azimuth β of the symmetry axis varies from layer to layer (Table 1), so the model does not have a through-going vertical symmetry plane. We performed 3-D anisotropic ray tracing and computed P-wave reflection traveltimes from the horizontal and dipping reflectors along four CMP lines oriented at azimuths 0°, 45°, 90°, and 135° with respect to the orientation of the dipping reflector. Then, we fit hyperbolas (3) to the computed traveltimes on conventional-length spreads and obtained azimuthally-varying effective moveout velocities. After approximating these velocities by the best-fit NMO ellipses (4), we used the generalized Dix formula (28) to calculate the interval ellipses (as described above) and carried out parameter estimation in each layer.

The inversion results are shown in Table 2. Since SV-wave reflections were not used in this test, we could not obtain the shear-wave symmetry-direction velocity V_{S0}. The errors in the medium parameters for all layers are rather small and mostly due to the influence of nonhyperbolic moveout on the finite-spread moveout velocity. Although we used an incorrect ("the best-guess") value of V_{S0} by assuming $V_{S0} = V_{P0}/2$, V_{S0} has a practically negligible influence on P-wave moveout. To verify this conclusion again, we carried out the inversion for the third layer using the exact NMO ellipses [given by equation (5)], rather than the ones obtained from the exact traveltimes, and an incorrect $V_{S0} = 1.5$ km/s. The inversion result in this case was almost perfect: $V_{P0} = 2.98$ km/s, $\epsilon = 0.31$, $\delta = 0.16$, $\nu = 39.8°$, and $\beta = 60.3°$ (compare to the last lines in Tables 1 and 2).

Nonhyperbolic moveout, caused by both vertical heterogeneity and anisotropy, introduces distortions into the moveout velocity†, which propagate into the interval NMO ellipses after being amplified by the Dix differentiation (28). The maximum deviations of the interval NMO velocities from the exact ellipses, however, are quite moderate [0.5%, 3.0%, and 1.9% for the first (subsurface), second, and third layer, respectively] and correspond to the horizontal events. Clearly, it is justified to use the hyperbolic moveout approximation for P-waves on conventional spreadlengths close to the distance between CMP and reflector.

It is interesting that while the largest error in the NMO velocity (3.0%) was observed in the second layer, the inversion results are least accurate for the bottom (third) layer (see Table 2). This is explained by the larger tilt ν of the symmetry axis in the second layer (60° compared to 40° in the third layer), which makes the inverted parameters less sensitive to errors in the input data. Indeed, the scatter of the inversion results in Figures 4c –

† The azimuthal variation of the fourth-order (quartic) moveout term is not an ellipse; in a horizontal layer, it is described by a quartic oval curve (Sayers and Ebrom, 1997).

4f is substantially smaller for the tilt $\nu = 60^\circ$ than that for $\nu = 40^\circ$.

Overall, the accuracy of the inversion in vertically heterogeneous TTI media can be predicted on the basis of the single-layer error analysis with a correction that takes into account the amplification of errors inherent in the Dix-type layer stripping.

Discussion and conclusions

We showed that the NMO ellipses of reflection events obtained from 3-D (azimuthal) moveout analysis can be used to determine the parameters of layered transversely isotropic media with a tilted axis of symmetry (TTI). For P-waves, reflection moveout and all other kinematic signatures in TTI media depend on five parameters – the symmetry-direction P-wave velocity V_{P0}, anisotropic coefficients ϵ and δ, and the orientation (tilt ν and azimuth β) of the symmetry axis. Since each NMO ellipse provides us with up to three equations for the medium parameters, the inversion procedure requires at least two ellipses for different reflection events. By developing the weak-anisotropy approximation and performing numerical inversion based on the exact NMO equation, we showed the feasibility of parameter estimation for the most common case of a horizontal and a dipping reflector. It should be emphasized that since the moveout inversion yields all parameters responsible for P-wave kinematics, conventional-spread surface reflection data contain enough information to perform *depth* processing in TTI media.

Stable inversion for all parameters, however, is impossible unless the symmetry-axis orientation, ϵ and δ satisfy several constraints. For instance, for vertical transverse isotropy ($\nu = 0$) P-wave reflection moveout depends on just two combinations of medium parameters – the zero-dip NMO velocity and the anisotropic coefficient η close to the difference between ϵ and δ (Alkhalifah and Tsvankin, 1995; Grechka and Tsvankin, 1996). Therefore, it is not surprising that the P-wave NMO ellipses become insensitive to the individual values of V_{P0}, ϵ, and δ for relatively mild tilts of the symmetry axis. Our numerical results show that if $\nu < 35 - 40^\circ$, the dip dependence of NMO velocity allows us to estimate only a combination of ϵ and δ close to η.

Also, the medium parameters cannot be found in a stable way if the reflector dip ϕ is less than about 30° (Figure 5) and the dip-dependent terms are not large enough for the anisotropic inversion. A similar minimum dip requirement in the P-wave moveout inversion was obtained for VTI media by Alkhalifah and Tsvankin (1995) and for HTI media by Contreras et al. (1997). Although the inversion becomes more stable with increasing dip, for dips approaching 70-80° specular reflections in a homogeneous medium may not exist at all. Yet another constraint should be satisfied by ϵ and δ: if the difference between ϵ and δ is small, the medium approaches elliptically anisotropic ($\epsilon = \delta$), and the moveout data can provide only the NMO ellipse for horizontal events and an estimate of $(\epsilon - \delta)$.

Thus, determination of the individual values of all parameters of TTI media responsible for P-wave velocity is possible only if both the tilt of the symmetry axis and reflector dip exceed 30-40°, and the medium is not close to elliptical. Even if some of these conditions are not satisfied, we may still be able to obtain certain parameter combinations (e.g., the parameter η for small tilts ν), but the inversion results will not be sufficient to carry out depth imaging.

A natural way to enhance the stability of the parameter estimation is to include NMO velocities of shear waves into the inversion procedure. The addition of the SV-wave NMO ellipse from a horizontal reflector helps to increase the accuracy of the inversion since the SV-wave moveout depends on only one extra parameter (the symmetry-direction shear velocity V_{S0}). Also, combining SV reflections from a horizontal interface with the P-wave NMO ellipses for a horizontal and a dipping reflector makes it possible to determine the parameters of elliptically anisotropic media. Still, including horizontal SV events is not sufficient to overcome the above constraints on the tilt of the symmetry axis and reflector dip. For instance, to determine the medium parameters for vertical transverse isotropy or mild tilts ν, it is necessary to use reflection moveout of SV or converted waves from *dipping* reflectors; this will be discussed in detail in a sequel paper.

Extension of our inversion scheme to vertically heterogeneous TTI media is based on the generalized Dix equation (Tsvankin et al., 1997), which expresses the NMO velocity through the matrices responsible for the interval NMO ellipses. As a result of the Dix-type layer stripping, we obtain the interval NMO ellipse, which can be inverted for the medium parameters using the single-layer algorithm. This inversion methodology was successfully tested on a synthetic data set generated by 3-D anisotropic ray tracing in a multilayered TTI model with depth-varying azimuth and tilt of the symmetry axis.

The TI model with a tilted symmetry axis discussed here should be rather common in overthrust areas (such as the Canadian Foothills) and near salt domes. Our inversion methodology provides an efficient way of estimating the anisotropic parameters needed for seismic imaging in these important exploration areas.

Acknowledgments

We are grateful to Ken Larner and Albena Mateeva

(Center for Wave Phenomena, Colorado School of Mines) for the review of this manuscript.

References

Alkhalifah, T., and Tsvankin, I., 1995, Velocity analysis in transversely isotropic media: Geophysics, **60**, 1550–1566.

Contreras, P., Grechka, V., and Tsvankin, I., 1997, Moveout inversion of P-wave data for horizontal transverse isotropy: Colorado School of Mines, Center for Wave Phenomena, Project Review, 93–103.

Dix, C.H., 1955, Seismic velocities from surface measurements: Geophysics, **20**, 68–86.

Grechka, V., and Tsvankin, I., 1996, 3-D description of normal moveout in anisotropic media: 66th Ann. Internat. Mtg., Soc. Expl. Geophys., Expanded Abstracts, 1487–1490.

Grechka, V. and Tsvankin, I., 1997, Moveout velocity analysis and parameter estimation for orthorhombic media: 67th Ann. Internat. Mtg., Soc. Expl. Geophys., Expanded Abstracts, 1226–1229.

Levin, F.K., 1971, Apparent velocity from dipping interface reflections: Geophysics, **36**, 510–516.

Sayers, C.M., and Ebrom, D.A., 1997, Seismic traveltime analysis for azimuthally anisotropic media: 67th Ann. Internat. Mtg., Soc. Expl. Geophys., Expanded Abstracts, 1238–1241.

Taner, M.T., and Koehler, F., 1969, Velocity spectra – digital computer derivation and application of velocity functions: Geophysics, **34**, 859–881.

Thomsen, L., 1986, Weak elastic anisotropy: Geophysics, **51**, 1954–1966.

Thomsen, L., 1988, Reflection seismology over azimuthally anisotropic media: Geophysics, **53**, 304–313.

Tsvankin, I., 1995, Normal moveout from dipping reflectors in anisotropic media: Geophysics, **60**, 268–284.

Tsvankin, I., 1996, P-wave signatures and notation for transversely isotropic media: An overview: Geophysics, **61**, 467–483.

Tsvankin, I., 1997a, Reflection moveout and parameter estimation for horizontal transverse isotropy: Geophysics, **62**, 614–629.

Tsvankin, I., 1997b, Moveout analysis for transversely isotropic media with a tilted symmetry axis: Geophysical Prospecting, **45**, 479–512.

Tsvankin, I., Grechka, V., and Cohen, J.K., 1997, Generalized Dix equation and modeling of normal moveout in inhomogeneous anisotropic media: 67th Ann. Internat. Mtg., Soc. Expl. Geophys., Expanded Abstracts, 1246–1249.

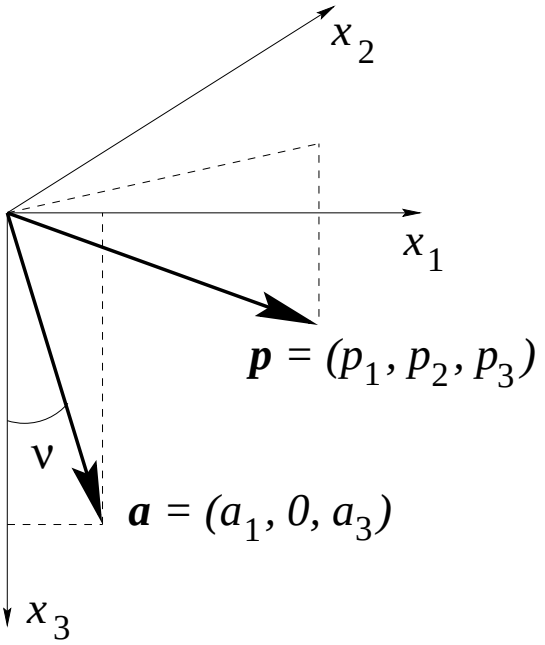

Figure A1. In the derivation of the weak-anisotropy approximation, the symmetry axis (described by the unit vector **a**) is assumed to be confined to the $[x_1, x_3]$-plane.

Tsvankin, I., and Thomsen, L., 1994, Nonhyperbolic reflection moveout in anisotropic media: Geophysics, **59**, 1290–1304.

Tsvankin, I., and Thomsen, L., 1995, Inversion of reflection traveltimes for transverse isotropy: Geophysics, **60**, 1095–1107.

Uren, N.F., Gardner, G.N.F., and McDonald, J.A., 1990, Normal moveout in anisotropic media: Geophysics, **55**, 1634–1636.

APPENDIX A: P-wave NMO ellipse in a weakly anisotropic TTI layer

The matrix **W** [equation (5)] that determines the NMO ellipse can be linearized with respect to the anisotropic coefficients ϵ and δ under the assumption of weak anisotropy ($|\epsilon| \ll 1$ and $|\delta| \ll 1$). Without losing generality, we assume that the symmetry axis (unit vector **a**) lies within the coordinate plane $[x_1, x_3]$ (Figure A1). Then

$$\mathbf{a} \equiv [a_1, 0, a_3] = [\sin\nu, 0, \cos\nu], \tag{A1}$$

where ν is the tilt of the axis.

To obtain the elements of the matrix **W**, we need to solve the Christoffel equation for the vertical component of the slowness vector $q \equiv p_3$ as a function of the horizontal slowness components p_1 and p_2. The Christoffel

equation for TI media can be written as

$$F \equiv (c_{11}s^2 + c_{44}c^2 - 1)\,(c_{44}s^2 + c_{33}c^2 - 1) - (c_{13} + c_{44})^2 s^2 c^2 = 0\,, \qquad \text{(A2)}$$

where $s = |\mathbf{p}|\sin\theta$ and $c = |\mathbf{p}|\cos\theta$; θ is the angle between the slowness vector $\mathbf{p}$ and the symmetry axis $\mathbf{a}$. Expressing s and c through the components of the vectors $\mathbf{p}$ and $\mathbf{a}$, we find

$$s^2 \equiv [\mathbf{a}\times\mathbf{p}]\cdot[\mathbf{a}\times\mathbf{p}] = p_2^2 + (a_3p_1 - a_1q)^2$$

and

$$c^2 \equiv (\mathbf{a}\cdot\mathbf{p})^2 = (a_1p_1 + a_3q)^2\,.$$

Next, we replace the stiffness coefficients c_{ij} with Thomsen (1986) parameters defined with respect to the symmetry axis:

$$c_{33} = \rho V_{P0}^2\,, \quad c_{44} = \rho V_{S0}^2\,, \quad c_{11} = \rho V_{P0}^2(1+2\epsilon)\,,$$
$$c_{13} = \rho\sqrt{(V_{P0}^2 - V_{S0}^2)\,(V_{P0}^2(1+2\delta) - V_{S0}^2)} - \rho V_{S0}^2\,, \qquad \text{(A3)}$$

and ρ is the density.

The linearized solution of the Christoffel equation (A2) for the vertical slowness q can be represented as the sum of the "isotropic" value $\tilde{q}$ and the correction term Δq due to the influence of anisotropy:

$$q \equiv p_3 = \tilde{q} + \Delta q\,. \qquad \text{(A4)}$$

For P-waves, the vertical slowness in isotropic media is given by

$$\tilde{q} = \sqrt{\frac{1}{V_{P0}^2} - p_1^2 - p_2^2}\,. \qquad \text{(A5)}$$

Δq can be considered as the linear term in a Taylor series expansion of q in ϵ and δ for fixed horizontal slownesses p_1 and p_2:

$$\Delta q = -\frac{1}{\partial F/\partial p_3}\left(\frac{\partial F}{\partial \epsilon}\,\epsilon + \frac{\partial F}{\partial \delta}\,\delta\right)\,, \qquad \text{(A6)}$$

with the partial derivatives obtained by differentiating the Christoffel equation (A2), $F = 0$. Combining equations (A4), (A5) and (A6) yields q as a function of p_1 and p_2 in weakly anisotropic TTI media.

Now we can obtain the derivatives $q_{,i} = \partial q/\partial p_i$ and $q_{,ij} = \partial^2 q/\partial p_i \partial p_j$, $(i,j = 1,2)$ from equation (A4) and substitute them into the exact equation (5) for the matrix $\mathbf{W}$. Further linearization of $\mathbf{W}$ in the anisotropic parameters using symbolic software Mathematica leads to the following final result:

$$W_{11} = \frac{1}{V_{P0}^2}\left(1 - 2\delta + 2\epsilon a_1^2 - 14\,(\epsilon-\delta)\,a_1^2a_3^2\right) - p_1^2 + \hat{W}_{11}(\epsilon-\delta)\,,$$
$$W_{12} = -p_1p_2 + \hat{W}_{12}(\epsilon-\delta)\,, \qquad \text{(A7)}$$

and

$$W_{22} = \frac{1}{V_{P0}^2}\left(1 - 2\delta - 2\,(\epsilon-\delta)\,a_1^2\,(1+a_3^2)\right) - p_2^2 + \hat{W}_{22}(\epsilon-\delta)\,.$$

In equations (A7), $y_1 = p_1^2V_{P0}^2$, $y_2 = p_2^2V_{P0}^2$, and

$$\begin{aligned}
\hat{W}_{11} &= 2p_1^2(-6 + 9y_1 - 4y_1^2)\,(1 - 8a_1^2a_3^2) \\
&\quad + 8a_1a_3p_1\tilde{q}(1-2a_1^2)\,(3 - 7y_1 + 4y_1^2) \\
&\quad + 2p_2^4a_3^4V_{P0}^2(1-4y_1) \\
&\quad + 4p_2^2\left[a_3^2(1-4a_1^2)\,(-1 + 5y_1 + 4y_1^2)\right. \\
&\qquad \left. + 2a_1a_3^3p_1\tilde{q}V_{P0}^2(-3 + 4y_1)\right]\,, \\
\hat{W}_{12} &= 8p_1p_2\left[-y_2^2a_3^4 + y_2a_3^2(2 - 5a_1^2 - 2y_1(1-4a_1^2))\right. \\
&\qquad - a_3^2(1-4a_1^2) + y_1\,(2 - a_1^2 - 12a_1^2a_3^2) \\
&\qquad \left. - y_1^2(1 - 8a_1^2a_3^2)\right] \qquad \text{(A8)} \\
&\quad + 8a_1a_3p_2\tilde{q}\left[a_3^2(1 - y_2(1-4y_1)\,)\right. \\
&\qquad \left. - \,y_1\,(5 - 8a_1^2) + 4y_1^2(1-2a_1^2)\right]\,, \\
\hat{W}_{22} &= -4p_1^2a_3^2(1-4a_1^2) + 2p_1^2y_1 - 16p_1^2y_1a_1^2a_3^2 \\
&\quad + 8a_1a_3p_1\tilde{q}\left[a_3^2 - y_1(1-2a_1^2)\right. \\
&\qquad \left. - y_2(5a_1^2 - 4y_1(1-2a_1^2))\right] \\
&\quad + 4p_2^2\left[-3a_3^4 + 5y_1a_3^2(1-4a_1^2) - 2y_1^2(1-8a_1^2a_3^2)\right] \\
&\quad + 2p_2^2y_2a_3^2\left[9a_3^2 - 8y_1(1-4a_1^2) + 16a_1a_3p_1\tilde{q}V_{P0}^2\right] \\
&\quad - 8p_2^2y_2^2a_3^4\,.
\end{aligned}$$